Chemical-Potential-Dependent Gap Opening at the Dirac Surface States of Bi_2Se_3 Induced by Aggregated Substitutional Cr Atoms

Cui-Zu Chang,[1,2,3] Peizhe Tang,[1,2] Yi-Lin Wang,[3] Xiao Feng,[1,2,3] Kang Li,[2,3] Zuocheng Zhang,[1,2] Yayu Wang,[1,2] Li-Li Wang,[1,2,3] Xi Chen,[1,2] Chaoxing Liu,[4] Wenhui Duan,[1,2,*] Ke He,[1,2,3,†] Xu-Cun Ma,[1,2,3] and Qi-Kun Xue[1,2]

[1]*State Key Laboratory of Low-Dimensional Quantum Physics, Department of Physics, Tsinghua University, Beijing 100084, China*

[2]*Collaborative Innovation Center of Quantum Matter, Beijing, China*

[3]*Beijing National Laboratory for Condensed Matter Physics, Institute of Physics, Chinese Academy of Sciences, Beijing 100190, China*

[4]*Department of Physics, The Pennsylvania State University, University Park, Pennsylvania 16802-6300, USA*

(Received 30 July 2013; published 6 February 2014; corrected 10 February 2014)

With angle-resolved photoemission spectroscopy, gap opening is resolved at up to room temperature in the Dirac surface states of molecular beam epitaxy grown Cr-doped Bi_2Se_3 topological insulator films, which, however, show no long-range ferromagnetic order down to 1.5 K. The gap size is found decreasing with increasing electron-doping level. Scanning tunneling microscopy and first-principles calculations demonstrate that substitutional Cr atoms aggregate into superparamagnetic multimers in the Bi_2Se_3 matrix, which contribute to the observed chemical-potential-dependent gap opening in the Dirac surface states without long-range ferromagnetic order.

DOI: 10.1103/PhysRevLett.112.056801 PACS numbers: 73.20.At, 75.50.Pp, 75.75.-c, 75.30.Hx

Time-reversal (TR) invariant topological insulators (TIs) are a new class of topological matters whose topologically nontrivial property is induced by spin-orbit coupling and protected by TR symmetry [1]. A three-dimensional (3D) TI is characterized by gapless surface states with Dirac-cone-shaped band dispersion around TR invariant points of surface Brillouin zone [2]. Ferromagnetic ordering can break the TR symmetry of a 3D TI and open a gap at the Dirac point of the surface states [3]. Many novel quantum phenomena predicted in 3D TIs, e.g., topological magnetoelectric effect, image magnetic monopoles, and quantum anomalous Hall effect [3–6], result from the magnetically gapped Dirac surface states (DSS).

Doping magnetic impurities is a convenient approach to induce long-range ferromagnetic order in a semiconductor or insulator if exchange coupling between impurities far from each other could be built [7–10]. Many experimental studies, from angle-resolved photoemission spectroscopy (ARPES) to transport measurements, have been devoted to magnetically doped Bi_2Se_3 family TIs: Bi_2Se_3, Bi_2Te_3, and Sb_2Te_3, which are by far the most popular TI materials [11–16]. The experimental results, however, are inconsistent between different materials and measurement methods. In magnetically doped Bi_2Te_3 and Sb_2Te_3, transport and magnetization measurements have shown clear long-range ferromagnetic order in several cases [12,13], which leads to the observation of the quantum anomalous Hall effect, a representative quantum phenomenon predicted in magnetic TIs [6]. Magnetically induced gap opening at DSS, however, could not be resolved by ARPES in these materials due to the low Curie temperature (T_C) and small gap size. Bi_2Se_3 is presumably the most studied TI material for its large bulk gap and standard DSS [11]. Magnetic-doping-induced gap opening at DSS has been reported in several ARPES studies on magnetically doped Bi_2Se_3 with gap size varying from several tens to a hundred meV, implying a strong ferromagnetism [14,15]. However, transport and magnetization measurements could only show very small or no magnetic hysteresis in the systems, making the existence of long-range ferromagnetic order questionable and hindering further progress to various quantum effects [14–16]. In this Letter, aiming at solving the puzzle in magnetically doped TIs, we have investigated the relation between magnetism and surface state gap in molecular beam epitaxy (MBE)-grown Cr-doped Bi_2Se_3 by combining ARPES, transport measurements, scanning tunneling microscopy (STM), and first-principles calculations. Our results demonstrate that substitutional Cr atoms in Bi_2Se_3 form superparamagnetic multimers, each with rather high T_C but without long-range ferromagnetic order as a whole. It leads to gapped DSS observed in ARPES without macroscopic ferromagnetism shown in transport and magnetization measurements.

Cr-doped Bi_2Se_3 films are prepared by MBE on graphene-terminated silicon carbide (0001) (for ARPES and STM measurements) or sapphire (0001) substrates (for transport measurements) [17]. In *situ* ARPES measurements are taken with a Scienta SES-2002 analyzer and a Gammadata helium discharging lamp producing unpolarized He Iα photons ($h\nu = 21.218$ eV). STM experiments are performed at 4.2 K with a Unisoku low-temperature STM system. The density functional theory calculations are carried out using the Vienna *ab initio* simulation package (VASP) with Perdew-Burke-Ernzerhof type generalized gradient approximation for exchange and correlation [17–19].

We mainly use 8 quintuple (QL) thick films in this study. Such a thickness is more than enough for a Bi_2Se_3 film to enter the 3D TI regime since the gap induced by hybridization between top and bottom DSS can only be observed in 5 QL and thinner films [20]. On the other hand, compared with thicker films, the surface state peaks of 8 QL films are better resolved in ARPES due to more uniform thickness and quantization of bulk bands into quantum well states [20]. The phenomena shown in this Letter observed from 8 QL films are also seen in thicker samples [17].

Figure 1 displays ARPES gray-scale band maps (upper panels) and the corresponding energy distribution curves (EDCs) (lower panels) of an 8 QL Bi_2Se_3 film and an 8 QL $Bi_{1.96}Cr_{0.04}Se_3$ film measured at room temperature (RT). In the spectra for the Bi_2Se_3 film [Figs. 1(a) and 1(c)], the DSS and parabolic quantum-well states are clearly observed. The Dirac point manifests itself as a distinct protrusion in the spectrum around $\bar{\Gamma}$ point [indicated by a red arrow in Fig. 1(c)], exhibiting the gapless nature of DSS. With a small amount of Cr impurities doped in Bi_2Se_3 (2% of the cations) [Figs. 1(b) and 1(d)], the spectrum near Dirac point changes from a protrusion into a dip [indicated by a red arrow in Fig. 1(d)], clearly indicating a gap opened here with the gap size ~75 meV. The gap becomes larger with increasing Cr concentration, see Supplemental Material [17].

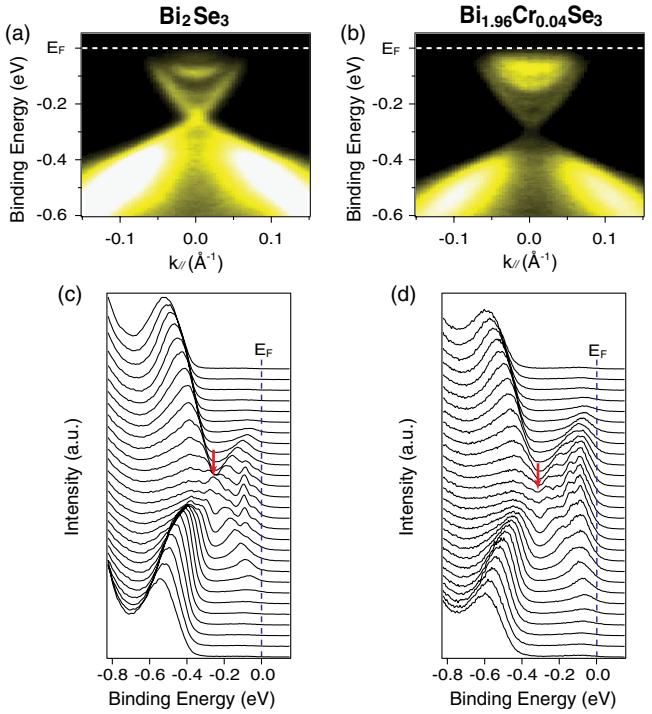

FIG. 1 (color online). ARPES gray-scale band maps (along the $\bar{\Gamma}$-$\bar{K}$ direction) (a),(b) and the corresponding EDCs (c),(d) of an 8 QL Bi_2Se_3 film (a),(c) and an 8 QL $Bi_{1.96}Cr_{0.04}Se_3$film (b),(d) taken at RT.

The 75 meV gap observed at RT suggests a rather strong ferromagnetism with T_C above RT induced by Cr doping. However, it is not supported by transport measurements. Figures 2(a) and 2(b) display magnetic field ($\mu_0 H$) dependence of the Hall resistance (R_{yx}) and longitudinal conductivity of an 8 QL $Bi_{1.96}Cr_{0.04}Se_3$ film, respectively, at varied temperature. Above 10 K, R_{yx} exhibits a linear relationship with $\mu_0 H$ and the magnetoconductance experiences a weak antilocalization behavior, both of which are characteristics of a TI with TR symmetry [21]. Below 10 K, a nonlinear Hall effect gradually develops, accompanied by the evolution of magnetoconductance to weak localization behavior. The observation implies breaking of TRS [22] by some magnetism which is also supported by direct magnetization measurement [17]. However, long-range ferromagnetic order is absent since no hysteresis is observed.

To probe the origin of the gap opening of DSS in the absence of long-range ferromagnetic order, we have systematically studied chemical potential (μ) dependence of the gap size (Δ) [1], because different magnetic coupling mechanisms have different μ dependence of their exchange energy which determines Δ [8–10]. The μ of Bi_2Se_3 can be tuned by doping Mg impurities [14,23] and by taking ARPES measurements at different temperatures through surface photovoltage effect [20,24]. Figures 3(a)–(c) show the ARPES EDCs of 8 QL $Bi_{1.96}Mg_yCr_{0.04}Se_3$ films with different Mg concentrations (y) measured at 150 K. In the film without Mg doping [Fig. 3(a)], the midgap energy (E_0) is −303 meV, and Δ is about 59 meV. The value of Δ is estimated by fitting the spectrum near the gap at $\bar{\Gamma}$point with double Lorentzian peaks, as shown in the inset of Fig. 3(g). Doping Mg to $y = 0.0015$ shifts E_0 to −275 meV with Δ increased to 85 meV [Fig. 3(b)]. As y is increased to 0.003 [Fig. 3(c)], E_0 is further shifted to −208 meV, whereas Δ is enhanced to 146 meV. Figures 3(d)–(f) show the ARPES EDCs of an 8 QL $Bi_{1.96}Cr_{0.04}Se_3$ film measured at different temperatures. At 80 K [Fig. 3(d)], the film is heavily electron doped with $E_0 = -403$ meV due to photoinduced electron doping [20,24]. The gap becomes so small that the surface states almost return to a gapless Dirac cone. At 150 K [Fig. 3(e)], with alleviative photoinduced doping, E_0 is shifted to −303 meV, whereas Δ is increased to 59 meV. At RT [Fig. 3(f)], E_0 reaches −280 meV, whereas

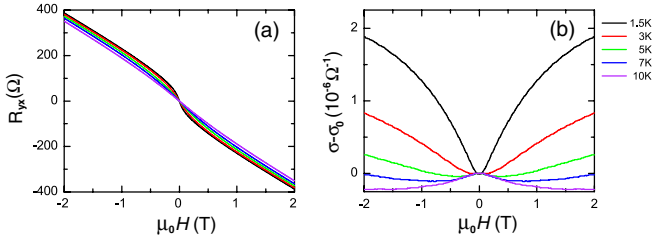

FIG. 2 (color online). Hall traces (a) and magnetoconductivity (b) of a 8 QL $Bi_{1.96}Cr_{0.04}Se_3$ film measured at varied temperatures.

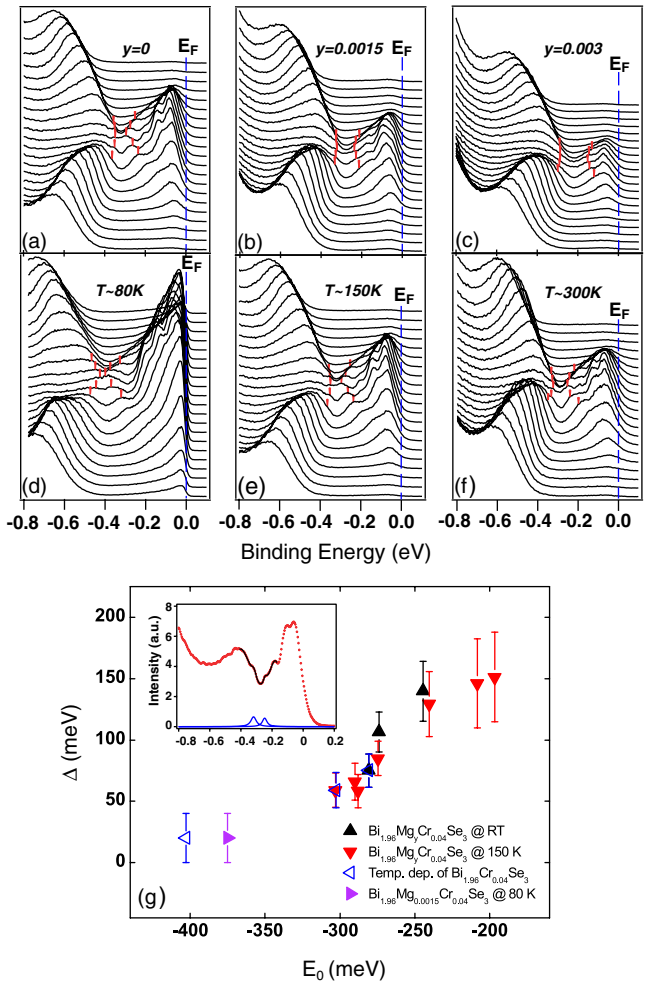

FIG. 3 (color online). (a)–(c) The ARPES EDCs of 8 QL $Bi_{1.96}Mg_yCr_{0.04}Se_3$ films taken at ~150 K with $y = 0$ (a), $y = 0.0015$ (b), and $y = 0.003$ (c). (d)–(f) The ARPES EDCs of an 8 QL $Bi_{1.96}Cr_{0.04}Se_3$ film taken at ~80 K (d), ~150 K (e), and ~300 K (f). (g) The relation between Δ and $|E_0|$ obtained from different ARPES measurements. The inset shows the fitting result of the $\bar{\Gamma}$ point spectrum of an 8 QL $Bi_{1.96}Cr_{0.04}Se_3$ film with double Lorentzian function.

Δ becomes ~75 meV. We have performed many ARPES measurements on samples with the same Cr doping level but different Mg concentrations at different temperatures. The data of Δ and $|E_0|$ obtained from the measurements (not limited to the spectra shown above) are plotted in Fig. 3(g). It is clear that Δ increases monotonically with decreasing $|E_0|$, regardless of the method applied to tune μ.

A sufficiently high Cr doping level can induce a transition of $Bi_{2-x}Cr_xSe_3$ from a TI to a topologically trivial insulator phase, which will destroy the DSS and ferromagnetism of van Vleck mechanism [25]. The Cr concentration of the samples studied here, however, is far below the critical value for such a topological phase transition ($x \sim 0.15$). The surface bands in the present samples still exist, only gapped around Dirac point, instead of being completely removed in topologically trivial phase [25]. Thus the above observations cannot be attributed to topological phase transition induced by Cr doping.

The measured μ dependence of gap size looks consistent with the Ruderman-Kittel-Kasuya-Yosida (RKKY)-like magnetic coupling mediated by DSS [9]. This surface RKKY ferromagnetism is enhanced when Fermi level approaches the Dirac point, and may not be detected by bulk-sensitive transport measurements since it only exists near the surface region. However, the T_C above RT is too high for RKKY-type ferromagnetism of a diluted magnetic system [9]. Surface-sensitive magnetic optic Kerr effect measurements also fail to detect any ferromagnetic signal from the Cr-doped Bi_2Se_3 films down to 10 K. Surface RKKY ferromagnetic coupling requires that the interimpurity distance be at least near the Fermi wavelength of the DSS. Longer distance leads to an exponential decrease of T_C [9]. From the ARPES data, the Fermi wavelength of DSS of $Bi_{1.96}Cr_{0.04}Se_3$ film is around 1 nm. As we will show below, it is much shorter than the average distance between Cr impurities (~6 nm). Therefore, the observed μ dependent gap opening cannot result from surface RKKY ferromagnetism.

We have performed STM measurements on Cr-doped Bi_2Se_3 to identify the configuration of Cr impurities in Bi_2Se_3 matrix. Figure 4(a) shows a typical STM image of an 8 QL $Bi_{1.96}Cr_{0.04}Se_3$ film. The terrace is scattered with defects (dark regions) resulting from Cr doping. Figure 4(b) shows a high-resolution STM image around one of the defects, which exhibits a polygonal shape in register with the surrounding lattice of Se atoms. The minimum-sized defects observed have an equilateral triangle shape covering three Se atoms, as shown in Fig. 4(c) (indicated by a black centered triangle). Similar to the look of magnetic impurities observed in Mn-doped Bi_2Te_3 and Cr-doped Sb_2Te_3 [12,13], the triangle-shaped defect can be attributed to a single substitutional Cr atom occupying subsurface Bi site (the center of the triangle), reducing the local density of states (DOS) of the three above Se atoms (the corners of the triangle). Larger defects can thus be attributed to multimers of several substitutional Cr atoms aggregated together. For example, the defect shown in Fig. 4(b) is composed of 8 substitutional Cr atoms, as indicated by 8 black centered triangles. It is different from Mn-doped Bi_2Te_3 and Cr-doped Sb_2Te_3 in which most impurities are triangle-shaped single substitutional defects away from each other [12,13].

We have used the first-principles calculations to investigate the properties of the multimers of substitutional Cr atoms. The simulated multimers contains three substitutional Cr atoms (trimers). There are two possible configurations of Cr trimers which are hereafter referred as C_1 and C_2, respectively, depending on the type of Se atoms locating in their centers [see the structural models shown in Figs. 4(d), 4(e), 4(h), and 4(i)]. In a Bi_2Se_3 QL, Bi, and Se atomic layers

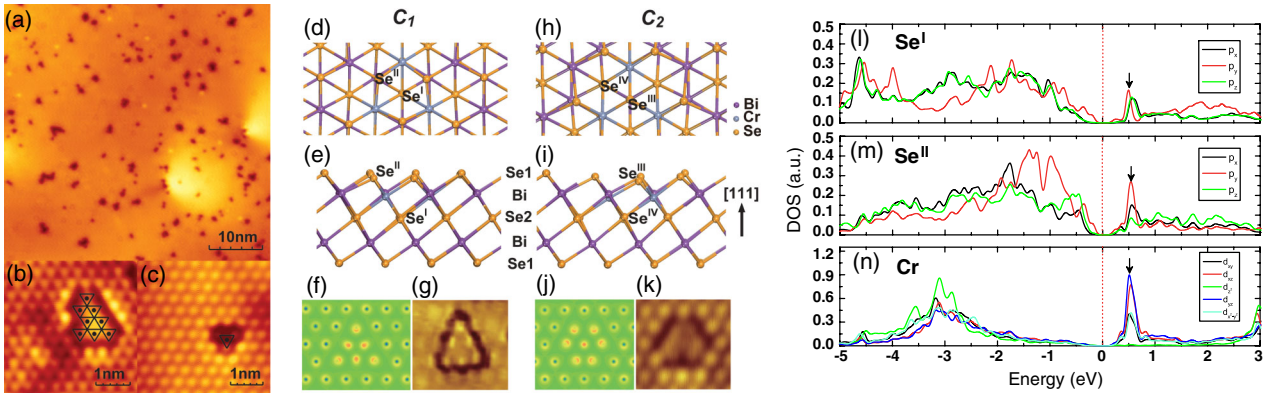

FIG. 4 (color online). (a)–(c) STM images of (50×50) nm (a), (3.8×3.8) nm (b), and (4×4) nm (c) taken from an 8 QL $Bi_{1.96}Cr_{0.04}Se_3$ film. (d),(e),(h),(i) Top (d),(h) and side (e),(i) views of the geometrical structures of C_1 (d),(e) and C_2 (h),(i) in a Bi_2Se_3 QL, respectively. (f),(g),(j),(k) Simulated (f),(j) and measured (g),(k) STM images of C_1 (f),(g) and C_2 (j),(k), respectively. (l)–(n) PDOS of Se^{I}, Se^{II}, and Cr atoms in C_1.

stack in the sequence of Se1-Bi-Se2-Bi-Se1 along the [111] direction [11]. C_1 and C_2 indicate the Cr trimers centered on Se atoms from Se2 [Se^{I} atom in Figs. 4(d) and 4(e)] and Se1 layers [Se^{III} atom in Figs. 4(h) and 4(i)], respectively. The two types of trimers have distinct charge density distributions in real space [as shown in Figs. 4(f) and 4(j)], both of which are observed by STM [see Figs. 4(g) and 4(k)].

The calculated formation energies of C_1 and C_2 trimers under Se-rich condition (the usual condition in MBE growth of Bi_2Se_3) are 1.155 and 1.158 eV, respectively, both much lower than that of isolated Cr substitution (1.323 eV) [17]. It explains why substitutional Cr atoms favor aggregation over dispersed distribution in Bi_2Se_3. The calculated projected DOS of $Se^{I}4p$, $Se^{II}4p$, and Cr3d orbitals of C_1 are shown in Figs. 4(l)–4(n), respectively. Because of crystal-field splitting, Cr3d orbitals are split into t_{2g} and e_g states: three electrons occupy the localized t_{2g} states and the unoccupied e_g state strongly hybrids with the p_y orbitals of Se^{I} and Se^{II} atoms. The strong p-d hybridization can induce ferromagnetism in each trimer, as observed in $Cd_{1-x}Mn_xTe_3$ [26] and $Zn_{1-x}Cr_xTe_3$ [27], through ferromagnetic superexchange mechanism [28]. C_2 has the similar situation with C_1 [17]. Energy-mapping analysis [29] shows that the ferromagnetic coupling strength between neighboring Cr ions is 24 and 29 meV for C_1 and C_2, respectively, corresponding to T_C near RT [30]. T_C above RT is expected in larger multimers. The calculated magnetic moment is 3 μ_B per Cr ion, consistent with SQUID measurements. The calculated magnetic anisotropy is perpendicular to film plane with the energy $K \sim 7.06 \times 10^6$ erg/cm^3.

It is difficult for the multimerized Cr impurities to build long-range ferromagnetic order because the intermultimer distance is too long for ferromagnetic coupling between them, no matter of surface RKKY or van Vleck mechanism. It means a superparamagnetic system composed of independent ferromagnetic multimers. The Hall traces in Fig. 2(a) indeed exhibit a typical superparamagnetic behavior with $T_B \sim 10$ K. From the T_B and the calculated magnetic anisotropy energy ($K \sim 7.06 \times 10^6$ erg/cm^3), the average size of multimers is estimated to be ~1 nm [27,31], in good agreement with the STM observations.

In superparamagnetism, the moment of a magnetic particle keeps flipping due to thermal fluctuation. However, the strong perpendicular magnetic anisotropy guarantees the magnetization of the Cr multimers perpendicular to the surface most of the time, no matter in spin-up or spin-down states. The DSS can be gapped near the Cr multimers in both of the spin states. Because of inhomogeneous magnetic doping, the DSS gap is not randomly distributed in real space, but with a finite correlation length. By using the effective disorder model (see the simulated result in Ref. [17]), we found that in the disorder configuration with a finite correlation length the total DOS is suppressed around Dirac point, which corresponds to the gap opening at DSS observed in ARPES.

Charging electrons into the Cr multimers can suppress their ferromagnetism according to our calculations [17] and reduce the gap size as observed by ARPES. For C_1, the charged electrons mainly locate at Se^{I} and Cr atoms and, due to Coulomb repulsion, induce a significant structural distortion: the bond lengths of Cr-Se^{I} and Cr-Se^{II} increase from 2.67 and 2.61 Å to 2.93 and 2.63 Å, respectively, and the bond angles of Cr-Se^{I}-Cr and Cr-Se^{II}-Cr change from 94.6° and 97.6° to 86.8° and 99.7°, respectively. This distortion weakens the ferromagnetic coupling between neighboring Cr ions from 24 to 16 meV, similar to the $Zn_{1-x}Cr_xTe_3$ case [27]. For C_2, the distribution of charged electrons is less localized and the induced Coulomb repulsion is not so strong; thus the ferromagnetism shows weaker μ dependence. Cr multimers larger than trimers usually contain at least one C_1 [17]. Therefore, μ dependence of gap opening can always be observed from the Cr-doped Bi_2Se_3 films.

Gapped DSS in the absence of long-range ferromagnetic order is a general phenomenon in magnetically doped Bi_2Se_3 that has long puzzled the researchers of TIs [14–16]. The present study demonstrates that the seeming contradiction comes from the short-range ferromagnetic order formed by aggregated magnetic dopants. The model proposed here can be directly applied to address magnetic doping in most chalcogenide TIs, a large class of the known TI materials [32]. Inhomogeneous magnetic doping is a common and crucial issue in traditional magnetic semiconductors and insulators, but has not yet received as much attention in magnetically doped TIs. This Letter first demonstrates how inhomogeneous magnetic doping influences and is influenced by the electronic properties of the host TI, which will help with the understanding of the existing and future experimental results on magnetically doped TIs. The magnetic nanodots embedded in a TI shown in this Letter also represents a new class of low-dimensional magnetic system in which the topological electronic properties of host material can be tuned by chemical potential via magnetism of nanodots. It promises new concept field effect devices for future electronic and spintronic applications.

C. C. and P. T. contributed equally to this work. We thank C. Wu, Z. Fang, X. Dai, K. Chang, X. L. Qi, S. C. Zhang, and L. Fu for helpful discussions. This work was supported by the National Natural Science Foundation of China, the Ministry of Science and Technology of China, and the Chinese Academy of Sciences.

*dwh@phys.tsinghua.edu.cn
†kehe@tsinghua.edu.cn

[1] M. Z. Hasan and C. L. Kane, Rev. Mod. Phys. **82**, 3045 (2010); X. -L. Qi and S. -C. Zhang, Rev. Mod. Phys. **83**, 1057 (2011).
[2] L. Fu, C. L. Kane, and E. J. Mele, Phys. Rev. Lett. **98**, 106803 (2007); D. Hsieh, D. Qian, L. Wray, Y. Xia, Y. S. Hor, R. J. Cava, and M. Z. Hasan, Nature (London) **452**, 970 (2008).
[3] X. -L. Qi, T. L. Hughes, and S. -C. Zhang, Phys. Rev. B **78**, 195424 (2008).
[4] X.-L. Qi, R. Li, J. Zang, and S.-C. Zhang, Science **323**, 1184 (2009).
[5] K. Nomura and N. Nagaosa, Phys. Rev. Lett. **106**, 166802 (2011).
[6] C. -Z. Chang *et al.*, Science **340**, 167 (2013).
[7] H. Ohno, D. Chiba, F. Matsukura, T. Omiya, E. Abe, T. Dietl, Y. Ohno, and K. Ohtani, Nature (London) **408**, 944 (2000); T. Dietl, Nat. Mater. **9**, 965 (2010).
[8] T. Dietl *et al.*, Science **287**, 1019 (2000).
[9] Q. Liu, C. X. Liu, C. Xu, X. L. Qi, and S. C. Zhang, Phys. Rev. Lett. **102**, 156603 (2009); G. Rosenberg and M. Franz, Phys. Rev. B **85**, 195119 (2012).
[10] R. Yu, W. Zhang, H.-J. Zhang, S.-C. Zhang, X. Dai, and Z. Fang, Science **329**, 61 (2010).
[11] H. Zhang, C.-X. Liu, X.-L. Qi, X. Dai, Z. Fang, and S.-C. Zhang, Nat. Phys. **5**, 438 (2009); Y. Xia *et al.*, Nat. Phys. **5**, 398 (2009).
[12] Y. J. Chien, Ph.D. thesis, University of Michigan, 2007 (http://deepblue.lib.umich.edu/handle/2027.42/57593); Y. S. Hor *et al.*, Phys. Rev. B **81**, 195203 (2010).
[13] C. -Z. Chang *et al.*, Adv. Mater. **25**, 1065 (2013).
[14] Y. L. Chen *et al.*, Science **329**, 659 (2010).
[15] S. -Y. Xu *et al.*, Nat. Phys. **8**, 616 (2012).
[16] Y. R. Song *et al.*, Appl. Phys. Lett. **100**, 242403 (2012); P. P. J. Haazen, J.-B. Laloë, T. J. Nummy, H. J. M. Swagten, P. Jarillo-Herrero, D. Heiman, and J. S. Moodera, Appl. Phys. Lett. **100**, 082404 (2012); D. Zhang *et al.*, Phys. Rev. B **86**, 205127 (2012).
[17] See Supplemental Material at http://link.aps.org/supplemental/10.1103/PhysRevLett.112.056801 for a detailed description on experimental and calculation methods and supporting data.
[18] G. Kresse and J. Furthmuller, Phys. Rev. B **54**, 11169 (1996).
[19] J. P. Perdew, K. Burke, and M. Ernzerhof, Phys. Rev. Lett. **77**, 3865 (1996).
[20] Y. Zhang *et al.*, Nat. Phys. **6**, 584 (2010).
[21] J. Chen *et al.*, Phys. Rev. Lett. **105**, 176602 (2010).
[22] M. Liu *et al.*, Phys. Rev. Lett. **108**, 036805 (2012); H. -Z. Lu, J. Shi, and S. Q. Shen, Phys. Rev. Lett. **107**, 076801 (2011).
[23] K. Kuroda *et al.*, Phys. Rev. Lett. **105**, 076802 (2010).
[24] D. Hsieh *et al.*, Nature (London) **460**, 1101 (2009).
[25] J. Zhang *et al.*, Science **339**, 1582 (2013).
[26] B. E. Larson, K. C. Hass, H. Ehrenreich, and A. E. Carlsson, Phys. Rev. B **37**, 4137 (1988).
[27] H. Saito, V. Zayets, S. Yamagata, and K. Ando, Phys. Rev. Lett. **90**, 207202 (2003); S. Kuroda, N. Nishizawa, K. Takita, M. Mitome, Y. Bando, K. Osuch, and T. Dietl, Nat. Mater. **6**, 440 (2007).
[28] J. Blinowski, P. Kacman, and J. A. Majewski, Phys. Rev. B **53**, 9524 (1996).
[29] Z. L. Li, J. H. Yang, G. H. Chen, M.-H. Whangbo, H. J. Xiang, and X. G. Gong, Phys. Rev. B **85**, 054426 (2012).
[30] K. Sato *et al.*, Rev. Mod. Phys. **82**, 1633 (2010).
[31] S. R. Shinde, S. Ogale, J. Higgins, H. Zheng, A. Millis, V. Kulkarni, R. Ramesh, R. Greene, and T. Venkatesan, Phys. Rev. Lett. **92**, 166601 (2004).
[32] B. Yan and S. -C. Zhang, Rep. Prog. Phys. **75**, 096501 (2012).